Artificial Graphene with Tunable Interactions

Thomas Uehlinger,[1] Gregor Jotzu,[1] Michael Messer,[1] Daniel Greif,[1,*] Walter Hofstetter,[2] Ulf Bissbort,[2,3] and Tilman Esslinger[1]

[1]*Institute for Quantum Electronics, ETH Zurich, 8093 Zurich, Switzerland*
[2]*Institut für Theoretische Physik, Johann Wolfgang Goethe-Universität, 60438 Frankfurt/Main, Germany*
[3]*Singapore University of Technology and Design, 138682 Singapore, Singapore*

(Received 15 August 2013; revised manuscript received 11 October 2013; published 31 October 2013)

We create an artificial graphene system with tunable interactions and study the crossover from metallic to Mott insulating regimes, both in isolated and coupled two-dimensional honeycomb layers. The artificial graphene consists of a two-component spin mixture of an ultracold atomic Fermi gas loaded into a hexagonal optical lattice. For strong repulsive interactions, we observe a suppression of double occupancy and measure a gapped excitation spectrum. We present a quantitative comparison between our measurements and theory, making use of a novel numerical method to obtain Wannier functions for complex lattice structures. Extending our studies to time-resolved measurements, we investigate the equilibration of the double occupancy as a function of lattice loading time.

DOI: 10.1103/PhysRevLett.111.185307 PACS numbers: 67.85.Lm, 71.10.Fd, 71.30.+h, 73.22.Pr

The engineering of systems that share their key properties with graphene [1], like Dirac fermions and a hexagonal structure, is gaining interest in an increasing number of disciplines in physics [2]. The artificial structures are created by confining photons in hexagonal lattices [3,4], by nanopatterning ultra-high-mobility two-dimensional electron gases [5], by scanning probe methods to assemble molecules on metal surfaces [6], and by trapping ultracold atoms in optical lattices [7,8]. The motivation for engineering graphenelike band structures is to explore regimes that are not, or not yet, accessible to research with graphene or similar materials. The artificial systems provide new avenues to topological [9,10] and quantum spin Hall insulators [11,12], as well as to intriguing strongly correlated phases [13]. To understand the role of interactions in solids with complex lattice structures [14], ultracold fermionic atoms in optical lattices are particularly promising, as the interparticle interactions and kinetic energy can be tuned [15,16], allowing for the realization of density and magnetic ordering [17–19]. In this Letter, we present and analyze a cold-atoms-based implementation of artificial graphene, where both the interaction and kinetic energy are tunable over a broad range. For strong interactions, we realize a 2D Mott insulator with ultracold fermions.

To obtain a quantum degenerate Fermi gas, we adhere to the procedure described in previous work [17]. A balanced spin mixture of ^{40}K atoms in the $m_F = -9/2$ and $-7/2$ magnetic sublevels of the $F = 9/2$ hyperfine manifold is evaporatively cooled in a crossed beam optical dipole trap to 15(2)% of the Fermi temperature. We prepare Fermi gases with total atom numbers between $N = 25 \times 10^3$ and 300×10^3, with 10% systematic uncertainty [20]. We either set the scattering length to $86(2)a_0$ using a Feshbach resonance or transfer to an $m_F = (-9/2, -5/2)$ mixture, where we access more repulsive interactions in the range of $a = 242(1)a_0$ to $632(12)a_0$ (the Bohr radius is denoted with a_0).

We then load the atoms into a tunable-geometry optical lattice [8] operating at a wavelength of $\lambda = 1064$ nm and consisting of three noninterfering, orthogonal standing-wave laser beams $\overline{X}$, Y, and $\tilde{Z}$. An additional beam X copropagates with $\overline{X}$ and interferes with Y; see Fig. 1. This gives rise to the potential

$$\begin{aligned} V(x,y,z) = &-V_{\overline{X}}\cos^2(k_L x + \theta/2) - V_X\cos^2(k_L x) \\ &- V_Y\cos^2(k_L y) - V_{\tilde{Z}}\cos^2(k_L z) \\ &- 2\alpha\sqrt{V_X V_Y}\cos(k_L x)\cos(k_L y)\cos\varphi, \end{aligned} \quad (1)$$

with $k_L = 2\pi/\lambda$, visibility $\alpha = 0.90(5)$, $\varphi = 0.00(3)\pi$, and $\theta = 1.000(1)\pi$. The phase φ between the interfering

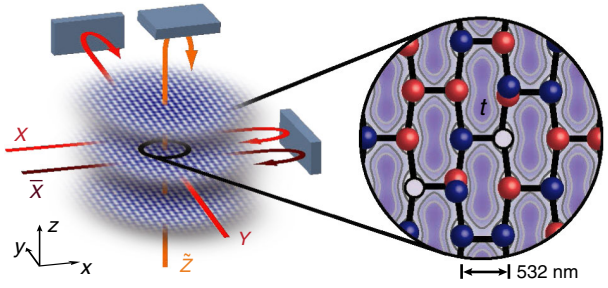

FIG. 1 (color online). Experimental setup used to create the artificial graphene system. Independent 2D layers of honeycomb geometry are realized using a tunable-geometry optical lattice. A sketch of the tunneling structure within the layers is shown on the right. The potential barriers between the sites are chosen such that the nearest-neighbor tunneling t in the hexagonal planes is equal along all bonds, resulting in a band structure containing two Dirac points [23]. A repulsively interacting two-component spin mixture of fermionic ^{40}K atoms (red and blue spheres) is loaded into the lattice. Gravity points along y.

beams X and Y is stabilized interferometrically, whereas the phase θ is controlled by the frequency difference between the beams X and $\overline{X}$. When tuning the lattice to a honeycomb geometry, Dirac points and their linear dispersion relation have been observed and characterized using Bloch-Zener transfers of noninteracting fermions, in excellent agreement with *ab initio* theory [8,21,22]. For the measurements presented in the following, the final lattice depths in units of the recoil energy are $V_{\overline{X},X,Y,\tilde{Z}}/E_R = [14.0(4), 0.79(2), 6.45(20), 30(1)]$, unless explicitly stated otherwise. All beams are ramped up simultaneously to their final intensities within 200 ms. The resulting potential contains several independent 2D honeycomb layers with a band structure containing two Dirac points [23]. The interlayer tunneling rate is below 2 Hz. For the combined external confining potential of the dipole trap and the lattice laser beams, we measure harmonic trapping frequencies of $\omega_{x,y,z}/2\pi = [86(2), 122(1), 57(1)]$ Hz.

We characterize the state of our system by measuring the fraction of atoms on doubly occupied sites D [17,20]. To determine D, the tunneling is suppressed by switching off V_X in roughly 5 μs and ramping up $V_{\overline{X}}$ and V_Y linearly to a depth of $30E_R$ within 500 μs. We then perform interaction dependent radio-frequency spectroscopy to obtain D [17]. Both the independently determined offset in D of 2.2(3)% due to an imperfect initial spin mixture as well as the calibrated detection efficiency of 89(2)% for double occupancies are taken into account [19].

In the experiment, we tune interactions from weakly $[U/3t = 1.8(3)]$ to strongly repulsive $[U/3t = 13(1)]$ and measure the double occupancy D as a function of the atom number N in the lattice; see Fig. 2(a). For weak interactions, the system is in a metallic state which is compressible, as signaled by an initial strong increase of D [24]. Here, creating more double occupancies requires less energy than placing additional atoms in the outside region of the harmonic trap where the potential energy is large. For high atom numbers, D saturates as the system enters a band insulating state. When increasing interactions, an incompressible Mott insulating state forms in the center of the trapped system. Therefore, D is strongly suppressed and does not increase as more atoms are added to the system. Only for the highest atom numbers does the chemical potential become comparable to the on-site interaction, allowing for the creation of double occupancies [17].

A quantitative comparison of our results with a microscopic theory is made possible by describing our system by the Fermi-Hubbard Hamiltonian

$$\hat{H} = -t\sum_{\langle ij\rangle,\sigma}(\hat{c}^{\dagger}_{i\sigma}\hat{c}_{j\sigma} + \text{H.c.}) + U\sum_{i}\hat{n}_{i\uparrow}\hat{n}_{i\downarrow} + \sum_{i,\sigma}V_i\hat{n}_{i\sigma}, \quad (2)$$

where $\hat{c}^{\dagger}_{i\sigma}$ and $\hat{c}_{i\sigma}$ denote the fermionic creation and annihilation operators for the two spin states $\sigma \in \{\uparrow,\downarrow\}$ and $\langle ij\rangle$ denotes nearest neighbors. The energy of the harmonic trap is V_i, and $\hat{n}_{i\sigma} = \hat{c}^{\dagger}_{i\sigma}\hat{c}_{i\sigma}$ is the density operator on site i. The determination of the on-site interaction energy U and the nearest-neighbor tunneling matrix element t requires an accurate calculation of the Wannier states, which is challenging for complex lattice structures such as those used in our experiment. To date, the Marzari-Vanderbilt scheme [25,26], which numerically minimizes the Wannier functions' spatial variance, has become well established in the solid state community and has recently also been used for optical lattices [27–29]. However, for complex lattice structures, a direct minimization may get stuck in local minima and becomes numerically expensive, requiring lattice-specific adaptations [28]. Instead, our numerical method (see Ref. [23]) is based on the alternative definition of Wannier states as eigenstates of band-projected position operators [30], which we show to be a

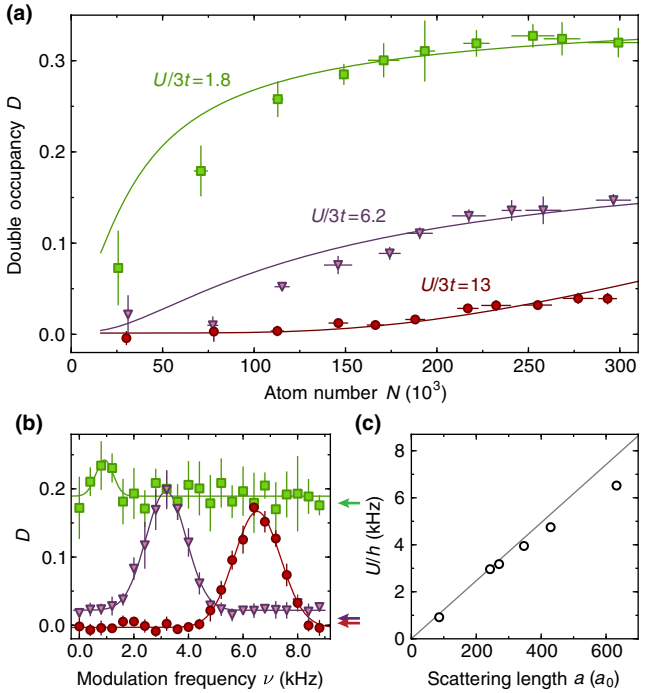

FIG. 2 (color online). Observing the metal to Mott insulator crossover in artificial graphene. (a) The measured double occupancy D versus atom number N for three different interaction strengths $U/3t$. For strong interactions, an incompressible Mott insulating core forms, leading to a strong suppression of D. Solid lines are theory predictions based on a high-temperature series expansion. (b) Excitation spectrum obtained by measuring D after sinusoidal modulation of the lattice depth V_Y for the same interaction strengths as above. The solid lines are Gaussian fits to the spectra. Arrows show the reference value without modulation. (c) Comparison of the extracted Hubbard parameters U with those obtained from a calculation of the Wannier functions in the honeycomb lattice. Error bars in D and N show the standard deviation of 5 measurements. In (c), the uncertainty in a and the fit error for the peak positions are smaller than the displayed data points. Data for additional interactions can be found in Ref. [23]. Negative values of D are caused by the subtraction of an independently measured offset.

very suitable starting point for a numerical procedure. The projection operator onto a subset of bands $\mathcal{A}$ can be written as $\mathcal{P}_{\mathcal{A}} = \sum_{\alpha\in\mathcal{A},\mathbf{k}} |\mathbf{k}, \alpha\rangle\langle\mathbf{k}, \alpha|$, where $|\mathbf{k}, \alpha\rangle$ is the 2D Bloch state with quasimomentum $\mathbf{k}$ in band α obtained from a standard band structure calculation of the lattice potential. The Wannier states are then given by the simultaneous eigenstates of the two operators $R_j = \mathcal{P}_{\mathcal{A}}(\mathbf{b}_j \cdot \hat{\mathbf{r}})\mathcal{P}_{\mathcal{A}}$ with $\hat{\mathbf{r}} = (\hat{x}, \hat{y})^T$ being real-space position operators, the reciprocal lattice vectors $\mathbf{b}_j$, and $j = 1, 2$. The calculation of the matrix elements $\langle\mathbf{k}, \alpha|R_j|\mathbf{k}', \alpha'\rangle$ via real-space integration can be performed analytically [23], reducing to a discrete summation of terms, which can be efficiently computed. In general, $\mathcal{A}$ contains as many bands as there are sites per unit cell, i.e., two for the honeycomb lattice. By finding the simultaneous eigenstates of these two position operators projected onto the lowest two bands, we explicitly obtain the maximally localized Wannier states. The tunneling between nearest neighbors and the interaction energy U is subsequently determined in the usual way from Wannier function overlap integrals [31]. Our method is extendible to inhomogeneous systems, generic to all dimensions, and allows proving the conjecture that the Wannier functions can be chosen to be real [23]. The method also holds for unit cells not symmetric under spatial reflection and if the Wannier states are no longer the Fourier transform of Bloch states.

We validate the qualitative interpretation of the data in Fig. 2(a) using a high-temperature series expansion up to second order of the grand canonical partition function [32] to determine the expected D. For the calculation, we use a nearest-neighbor tunneling of $t/h = 172(20)$ Hz within the layers (h is Planck's constant) and separately measured on-site interaction energies $U/h = [0.92(12), 3.18(2), 6.52(3)]$ kHz at the chosen scattering lengths $a = [86(2), 270(1), 632(12)]a_0$. The model assumes a connectivity of 3 within the 2D planes and no interlayer tunneling, as well as a globally thermalized cloud. Both finite temperature and the harmonic trap are taken into account. We obtain overall good agreement with theory when allowing for the entropy per atom in the lattice $s = S/N$ as a fit parameter [20]. For the three interactions, the fitted entropies of $s = [2.1, 2.7, 1.7]k_B$ are comparable to $s_{\text{in}} = 1.5(2)k_B$ and $s_{\text{out}} = 2.5(1)k_B$ measured in the dipole trap before loading and after reversing the loading procedure (k_B is the Boltzmann constant). From these parameters, we compute that about 50 layers contain Mott insulating cores, each of which consists of up to 2000 atoms. Deviations from theory are likely to arise because of incomplete thermalization. The tunneling time scale is expected to be sufficiently fast for equilibration within layers (see below). Yet, the slow interlayer tunneling when approaching the final configuration hinders the formation of a globally thermalized state. A more detailed analysis would require a full nonequilibrium model of coupled 2D layers.

A characteristic feature of a Mott insulator is a gapped excitation spectrum [33], which we probe by recording D in response to modulating the lattice depth at different frequencies ν [17]. After loading the gas into the lattice, we sinusoidally modulate V_Y for 40 ms by $\pm 10\%$. As V_Y interferes with V_X, this leads to a modulation in tunneling t_x (t_y) of $\sim \pm 7\%$ ($\mp 17\%$) as well as an additional modulation of U by $\pm 3\%$ caused by the changing width of the Wannier functions. For all potentials sampled during the modulation, the Dirac points are retained in the band structure, as $t_x < 2t_y$ [21]. For the whole parameter range, the response of the system is within the linear regime of double occupancy creation [34], where the creation rate is proportional to the energy absorption rate [35]. In Fig. 2(b), we plot both the response and the measured base level without modulation (arrows) for the same interactions as used in Fig. 2(a) and $N = 80(2) \times 10^3$. For weak interactions, there is almost no detectable response. When entering the Mott insulating regime, we observe a gapped spectrum with a pronounced peak at $\nu = U/h$, corresponding to the creation of localized double occupancies.

In Fig. 2(c), we compare the peak position at $\nu = U/h$ obtained from Gaussian fits to modulation spectra for various scattering lengths [23] with the on-site interaction energy calculated using Wannier functions. For weak interactions, the *ab initio* calculation of the Hubbard parameter U agrees well with the measured value [see also Fig. 4(d)]. Deviations are observed for the strongest interactions. We attribute this effect to the deep optical lattice in one direction leading to a size of the Wannier function comparable to the scattering length and possibly higher band effects. A more detailed theory would, however, be necessary for a quantitative comparison in this regime.

The equilibration within the 2D honeycomb layers requires a change of the quantum many-body state during the lattice loading process. This is determined by the time necessary for the global density redistribution and the formation of correlations associated with the change in external potential. So far, equilibration dynamics have been investigated experimentally for bosonic atoms in optical lattices [36–38], whereas for strongly correlated fermions, the time evolution from the continuum to the Hubbard regime has not been studied yet. In Fig. 3, we study the lattice loading process by measuring the resulting D after an S-shaped intensity ramp [23] lasting between $\tau_L = 5$ ms and $\tau_L = 600$ ms. Both for intermediate [$a = 242(1)a_0$] and strong interactions [$a = 632(12)a_0$], we observe a fast rise of D within roughly 200 ms followed by a slow decay. We additionally plot the expected D as derived from the high-temperature series expansion (solid line), assuming global thermal equilibrium and taking into account atom loss and an independently determined heating rate [23]. For $\tau_L \gtrsim 200$ ms, the measured double occupancy agrees with the theoretical model. When comparing this time scale with the nearest-neighbor tunneling time of 6 ms in the honeycomb

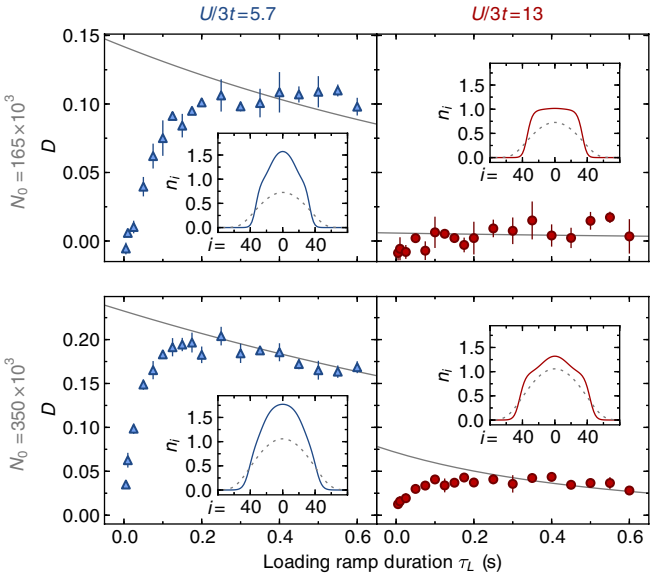

FIG. 3 (color online). The lattice loading process. The panels show D after loading ramps with varying duration τ_L for two interactions and two initial atom numbers. The solid line is the expected D from the high-temperature series expansion, taking atom loss and heating during lattice loading into account [23]. The insets show the calculated equilibrium density profiles for the atomic cloud in the optical dipole trap (dashed lines) and in the lattice (solid lines), illustrating the required density redistribution during the loading. Here, the initial atom number and entropies before loading into the lattice were used. Error bars in D show the standard deviation of 3 measurements.

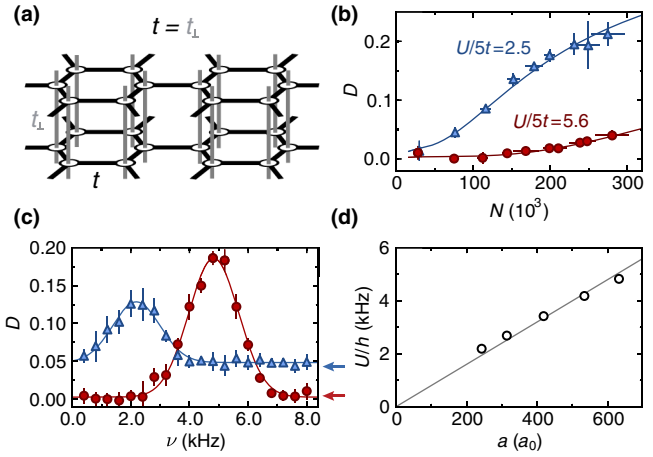

FIG. 4 (color online). Coupled layers of artificial graphene. (a) Detail of the coupled-layer structure with $t = t_\perp$. The atoms populate about 80 layers. (b) The double occupancy D versus atom number N in the metallic and Mott insulating regime. Solid lines are theory predictions based on a high-temperature series expansion. (c) Excitation spectra for the interactions used in (b). The solid lines are Gaussian fits to the spectra. Arrows show the reference value without modulation. (d) The on-site interaction energy U compared to the theoretical expectation. Error bars are as in Fig. 2. Data for additional interactions can be found in Ref. [23].

layers, this suggests that 200 ms is sufficient for density redistribution within the 2D layers (for the case of coupled layers, similar time scales are observed [23]). The calculated density profiles for different interactions and atom numbers (insets of Fig. 3) indicate that the core density has to increase when loading the atoms from the dipole trap into the lattice. For very short ramp times, this density redistribution cannot occur, leading to densities in the trap center, which are too low. This is confirmed by the observed low values of D as compared to theory for small τ_L.

The coupling between 2D layers is known to alter their physical properties as compared to monolayer systems. For the case of real graphene, this has been used to modify the dispersion relation around the Dirac points [39]. In our experiment, coupled honeycomb layers stacked as shown in Fig. 4(a) can be produced, opening the possibility to simulate multilayer systems with tunable interactions. The tunneling between sites of adjacent layers $t_\perp$ can be controlled via the lattice depth $V_{\tilde{Z}}$. In the following, we set $V_{\tilde{Z}} = 7E_R$ (corresponding to $t = t_\perp$) and investigate the dependence of double occupancy on atom number; see Fig. 4(b). The scattering length is set to the same values as in Fig. 3, and $\omega_{x,y,z}/2\pi = [55.7(7), 106(1), 57(1)]$ Hz. For weak repulsive interactions [$U/5t = 2.5(3)$ with $U/h = 2.18(4)$ kHz], the system is metallic, whereas for large interactions [$U/5t = 5.6(7)$ with $U/h = 4.82(2)$ kHz], the half-filled system is in the Mott insulating regime, signaled by a strong suppression of D. We find excellent agreement with the theoretical predictions of the high-temperature series expansion using a connectivity of 5. The fitted entropy per particle is $s = 1.8k_B$ for both interactions. As compared to the 2D measurements, we find only negligible deviations from the calculated double occupancy for the whole range of interactions [23]. We attribute this to the fast tunneling time between layers, leading to equilibration even between the honeycomb planes.

Both the uncoupled- and coupled-layer systems show a crossover from the metallic to the Mott insulating regime. However, quantitative differences are observed in the double occupancy dependence for the case of coupled layers. These differences originate in the altered lattice structure, which changes both the lattice connectivity and on-site interaction U. Using the same method as for the 2D data, we measure the lattice modulation spectra and find a reduction by about 25% for the value of U at the same scattering length; see Fig. 4(c). For strong interactions, a gapped excitation spectrum is found, as expected for a Mott insulating state. The experimentally determined U is shown in Fig. 4(d). In contrast to the 2D measurements, it does not deviate from the results obtained from lowest-band Wannier function overlap integrals even for the largest scattering lengths, owing to the weaker lattice depth along the coupled-layer direction.

In conclusion, we have investigated the properties of an artificial graphene system as a function of interactions.

Mapping to a microscopic theory has provided insight into equilibration dynamics and the effect of coupling layers. The realization of a two-dimensional fermionic Mott insulator provides a platform for studying further strongly correlated phases, which have attracted particular interest in the honeycomb geometry, where spin-liquid and superconducting phases have been predicted [13,40,41].

We would like to thank Hari Manoharan and Leticia Tarruell for insightful discussions. We acknowledge SNF, NCCR-QSIT, and SQMS (ERC Advanced Grant) for funding. U. B. and W. H. acknowledge support from SFB-TR/49 and Forschergruppe FOR 801 by the DFG.

*greif@phys.ethz.ch

[1] A. H. Castro Neto, F. Guinea, N. M. R. Peres, K. S. Novoselov, and A. K. Geim, Rev. Mod. Phys. **81**, 109 (2009).
[2] M. Polini, F. Guinea, M. Lewenstein, H. C. Manoharan, and V. Pellegrini, Nat. Nanotechnol. **8**, 625 (2013).
[3] O. Peleg, G. Bartal, B. Freedman, O. Manela, M. Segev, and D. N. Christodoulides, Phys. Rev. Lett. **98**, 103901 (2007).
[4] U. Kuhl, S. Barkhofen, T. Tudorovskiy, H.-J. Stöckmann, T. Hossain, L. de Forges de Parny, and F. Mortessagne, Phys. Rev. B **82**, 094308 (2010).
[5] A. Singha, M. Gibertini, B. Karmakar, S. Yuan, M. Polini, G. Vignale, M. I. Katsnelson, A. Pinczuk, L. N. Pfeiffer, K. W. West, and V. Pellegrini, Science **332**, 1176 (2011).
[6] K. K. Gomes, W. Mar, W. Ko, F. Guinea, and H. C. Manoharan, Nature (London) **483**, 306 (2012).
[7] P. Soltan-Panahi, J. Struck, P. Hauke, A. Bick, W. Plenkers, G. Meineke, C. Becker, P. Windpassinger, M. Lewenstein, and K. Sengstock, Nat. Phys. **7**, 434 (2011).
[8] L. Tarruell, D. Greif, T. Uehlinger, G. Jotzu, and T. Esslinger, Nature (London) **483**, 302 (2012).
[9] F. D. M. Haldane, Phys. Rev. Lett. **61**, 2015 (1988).
[10] M. C. Rechtsman, J. M. Zeuner, Y. Plotnik, Y. Lumer, D. Podolsky, F. Dreisow, S. Nolte, M. Segev, and A. Szameit, Nature (London) **496**, 196 (2013).
[11] C. L. Kane and E. J. Mele, Phys. Rev. Lett. **95**, 226801 (2005).
[12] F. Guinea, M. I. Katsnelson, and A. K. Geim, Nat. Phys. **6**, 30 (2010).
[13] Z. Y. Meng, T. C. Lang, S. Wessel, F. F. Assaad, and A. Muramatsu, Nature (London) **464**, 847 (2010).
[14] V. N. Kotov, B. Uchoa, V. M. Pereira, F. Guinea, and A. H. Castro Neto, Rev. Mod. Phys. **84**, 1067 (2012).
[15] M. Lewenstein, A. Sanpera, V. Ahufinger, B. Damski, A. Sen(De), and U. Sen, Adv. Phys. **56**, 243 (2007).
[16] T. Esslinger, Annu. Rev. Condens. Matter Phys. **1**, 129 (2010).
[17] R. Jördens, N. Strohmaier, K. Günter, H. Moritz, and T. Esslinger, Nature (London) **455**, 204 (2008).
[18] U. Schneider, L. Hackermüller, S. Will, T. Best, I. Bloch, T. A. Costi, R. W. Helmes, D. Rasch, and A. Rosch, Science **322**, 1520 (2008).
[19] D. Greif, T. Uehlinger, G. Jotzu, L. Tarruell, and T. Esslinger, Science **340**, 1307 (2013).
[20] R. Jördens, L. Tarruell, D. Greif, T. Uehlinger, N. Strohmaier, H. Moritz, T. Esslinger, L. De Leo, C. Kollath, A. Georges, V. Scarola, L. Pollet, E. Burovski, E. Kozik, and M. Troyer, Phys. Rev. Lett. **104**, 180401 (2010).
[21] L.-K. Lim, J.-N. Fuchs, and G. Montambaux, Phys. Rev. Lett. **108**, 175303 (2012).
[22] T. Uehlinger, D. Greif, G. Jotzu, L. Tarruell, T. Esslinger, L. Wang, and M. Troyer, Eur. Phys. J. Special Topics **217**, 121 (2013).
[23] See Supplemental Material at http://link.aps.org/supplemental/10.1103/PhysRevLett.111.185307 for details on additional experimental data, the lattice loading procedure, the noninteracting band structure and our alternative method of calculating Wannier states.
[24] V. W. Scarola, L. Pollet, J. Oitmaa, and M. Troyer, Phys. Rev. Lett. **102**, 135302 (2009).
[25] N. Marzari and D. Vanderbilt, Phys. Rev. B **56**, 12 847 (1997).
[26] A. A. Mostofi, J. R. Yates, Y.-S. Lee, I. Souza, D. Vanderbilt, and N. Marzari, Comput. Phys. Commun. **178**, 685 (2008).
[27] J. Ibañez-Azpiroz, A. Eiguren, A. Bergara, G. Pettini, and M. Modugno, Phys. Rev. A **87**, 011602 (2013).
[28] R. Walters, G. Cotugno, T. H. Johnson, S. R. Clark, and D. Jaksch, Phys. Rev. A **87**, 043613 (2013).
[29] J. Ibañez-Azpiroz, A. Eiguren, A. Bergara, G. Pettini, and M. Modugno, Phys. Rev. A **88**, 033631 (2013).
[30] S. Kivelson, Phys. Rev. B **26**, 4269 (1982).
[31] D. Jaksch and P. Zoller, Ann. Phys. (Amsterdam) **315**, 52 (2005).
[32] J. Oitmaa, C. Hamer, and W. Zheng, *Series Expansion Methods for Strongly Interacting Lattice Models* (Cambridge University Press, Cambridge, England, 2006).
[33] W. F. Brinkman and T. M. Rice, Phys. Rev. B **2**, 1324 (1970).
[34] D. Greif, L. Tarruell, T. Uehlinger, R. Jördens, and T. Esslinger, Phys. Rev. Lett. **106**, 145302 (2011).
[35] A. Tokuno and T. Giamarchi, Phys. Rev. A **85**, 061603 (2012).
[36] T. Gericke, F. Gerbier, A. Widera, S. Fölling, O. Mandel, and I. Bloch, J. Mod. Opt. **54**, 735 (2007).
[37] C.-L. Hung, X. Zhang, N. Gemelke, and C. Chin, Phys. Rev. Lett. **104**, 160403 (2010).
[38] W. S. Bakr, A. Peng, M. E. Tai, R. Ma, J. Simon, J. I. Gillen, S. Fölling, L. Pollet, and M. Greiner, Science **329**, 547 (2010).
[39] K. S. Novoselov, E. McCann, S. V. Morozov, V. I. Fal'ko, M. I. Katsnelson, U. Zeitler, D. Jiang, F. Schedin, and A. K. Geim, Nat. Phys. **2**, 177 (2006).
[40] E. Zhao and A. Paramekanti, Phys. Rev. Lett. **97**, 230404 (2006).
[41] R. Nandkishore, L. S. Levitov, and A. V. Chubukov, Nat. Phys. **8**, 158 (2012).